WILLIAM & MARY
CHARTERED 1693

W&M ScholarWorks

Arts & Sciences Articles

Arts and Sciences

2015

Measurement of muon plus proton final states in nu(mu) interactions on hydrocarbon at < E-nu >=4.2 GeV

T. Walton

M. E. Christy

M. Datta

L. Aliaga
College of William and Mary

J. Devan
College of William and Mary

See next page for additional authors

Follow this and additional works at: https://scholarworks.wm.edu/aspubs

Recommended Citation

Authors

T. Walton, M. E. Christy, M. Datta, L. Aliaga, J. Devan, J. K. Nelson, A. Norrick, and D. Zhang

Measurement of muon plus proton final states in ν_μ Interactions on Hydrocarbon at $\langle E_\nu \rangle = 4.2$ GeV

T. Walton,[1, *] M. Betancourt,[2] L. Aliaga,[3, 4] O. Altinok,[5] A. Bodek,[6] A. Bravar,[7] H. Budd,[6]
M. J. Bustamante,[4] A. Butkevich,[8] D.A. Martinez Caicedo,[9, 2] M.F. Carneiro,[9] C.M. Castromonte,[9]
M.E. Christy,[1] J. Chvojka,[6] H. da Motta,[9] M. Datta,[1] J. Devan,[3] S.A. Dytman,[10] G.A. Díaz,[4] B. Eberly,[10, †]
J. Felix,[11] L. Fields,[12] R. Fine,[6] G.A. Fiorentini,[9] A.M. Gago,[4] H. Gallagher,[5] R. Gran,[13] D.A. Harris,[2]
A. Higuera,[6, 11] K. Hurtado,[9, 14] J. Kleykamp,[6] M. Kordosky,[3] S.A. Kulagin,[8] T. Le,[15] E. Maher,[16]
S. Manly,[6] W.A. Mann,[5] C.M. Marshall,[6] C. Martin Mari,[7] K.S. McFarland,[6, 2] C.L. McGivern,[10]
A.M. McGowan,[6] B. Messerly,[10] J. Miller,[17] A. Mislivec,[6] J.G. Morfín,[2] J. Mousseau,[18] T. Muhlbeier,[9]
D. Naples,[10] J.K. Nelson,[3] A. Norrick,[3] J. Osta,[2] V. Paolone,[10] J. Park,[6] C.E. Patrick,[12] G.N. Perdue,[2, 6]
L. Rakotondravohitra,[2, ‡] R.D. Ransome,[15] H. Ray,[18] L. Ren,[10] P.A. Rodrigues,[6] D. Ruterbories,[6]
H. Schellman,[12] D.W. Schmitz,[19, 2] C. Simon,[20] F.D. Snider,[2] J.T. Sobczyk,[2, §] C.J. Solano Salinas,[14] N. Tagg,[21]
B.G. Tice,[15, ¶] E. Valencia,[11] J. Wolcott,[6] M.Wospakrik,[18] G. Zavala,[11] D. Zhang,[3] and B.P.Ziemer[20]

(MINERvA Collaboration)

[1]Hampton University, Dept. of Physics, Hampton, VA 23668, USA
[2]Fermi National Accelerator Laboratory, Batavia, Illinois 60510, USA
[3]Department of Physics, College of William & Mary, Williamsburg, Virginia 23187, USA
[4]Sección Física, Departamento de Ciencias, Pontificia Universidad Católica del Perú, Apartado 1761, Lima, Perú
[5]Physics Department, Tufts University, Medford, Massachusetts 02155, USA
[6]University of Rochester, Rochester, New York 14610 USA
[7]University of Geneva, Geneva, Switzerland
[8]Institute for Nuclear Research of the Russian Academy of Sciences, 117312 Moscow, Russia
[9]Centro Brasileiro de Pesquisas Físicas, Rua Dr. Xavier Sigaud 150, Urca, Rio de Janeiro, RJ, 22290-180, Brazil
[10]Department of Physics and Astronomy, University of Pittsburgh, Pittsburgh, Pennsylvania 15260, USA
[11]Campus León y Campus Guanajuato, Universidad de Guanajuato, Lascurain
de Retana No. 5, Col. Centro. Guanajuato 36000, Guanajuato México.
[12]Northwestern University, Evanston, Illinois 60208
[13]Department of Physics, University of Minnesota – Duluth, Duluth, Minnesota 55812, USA
[14]Universidad Nacional de Ingeniería, Apartado 31139, Lima, Perú
[15]Rutgers, The State University of New Jersey, Piscataway, New Jersey 08854, USA
[16]Massachusetts College of Liberal Arts, 375 Church Street, North Adams, MA 01247
[17]Departamento de Física, Universidad Técnica Federico Santa María, Avda. España 1680 Casilla 110-V, Valparaíso, Chile
[18]University of Florida, Department of Physics, Gainesville, FL 32611
[19]Enrico Fermi Institute, University of Chicago, Chicago, IL 60637 USA
[20]Department of Physics and Astronomy, University of California, Irvine, Irvine, California 92697-4575, USA
[21]Department of Physics, Otterbein University, 1 South Grove Street, Westerville, OH, 43081 USA
(Dated: March 4, 2015)

A study of charged-current muon neutrino scattering on hydrocarbon (CH) in which the final state includes a muon, at least one proton, and no pions is presented. Although this signature has the topology of neutrino quasielastic scattering from neutrons, the event sample contains contributions from quasielastic and inelastic processes where pions are absorbed in the nucleus. The analysis accepts events with muon production angles up to 70° and proton kinetic energies greater than 110 MeV. The cross section, when based completely on hadronic kinematics, is well-described by a relativistic Fermi gas nuclear model including the neutrino event generator modeling for inelastic processes and particle transportation through the nucleus. This is in contrast to the quasielastic cross section based on muon kinematics, which is best described by an extended model that incorporates multi-nucleon correlations. This measurement guides the formulation of a complete description of neutrino-nucleus interactions that encompasses the hadronic as well as the leptonic aspects of this process.

---

*now at Fermi National Accelerator Laboratory, Batavia, IL 60510 USA

Neutrino quasielastic scattering $\nu_l N(n) \to l^- p$ on nuclei N is a dominant signal process for neutrino oscillation experiments and is used to extract information about the axial vector form factor for nucleons [1–5]. The simple final-state topology combined with an assumption that the initial-state nucleon is at rest allows for an estimate of the neutrino energy from the final-state lepton kinematics alone. This estimate can be altered by the fact that the nucleon is bound in a nucleus, which is often modeled by assuming that the nucleons are non-interacting within a relativistic Fermi gas (RFG). However, measurements based on the final-state lepton on nuclei with A > 2 over different ranges of four-momentum transfer Q^2 are inconsistent with the RFG model with $M_A \sim 1$ GeV in the absolute size of the cross section per nucleon and the predicted energy deposition near the vertex of these interactions [1, 2, 5–8].

Many models of nuclear effects attempt to explain these discrepancies by considering possible correlations between nucleons. These include short-range correlations as observed in electron scattering [9–11], long-range correlations that are modeled with the random phase approximation (RPA) [12–16], and meson exchange currents (MEC) [15–21]. Each of these processes changes the event rate and final-state particle kinematics.

In addition, hadrons produced in neutrino-nucleus interactions can undergo final-state interactions (FSI) as they propagate through the nucleus. Consequently, a sample including only a lepton and nucleons will invariably contain events from inelastic processes. These include $\Delta(1232)$ resonance production and decay, where the pion is not observed. Events from both inelastic processes with no final-state pions and nucleon-nucleon correlations contribute to the measured quasielastic (QE) cross section, but have different kinematics and final-state hadron content for the same neutrino energy. Therefore, these events can alter the accuracy of any neutrino energy estimate [22–28] that neutrino oscillation experiments [29, 30] use.

Additional information is accessible through measurements of the hadronic component. Previous measurements [1, 3–5] have made a selection on the energy and/or direction of a tracked proton and its consistency with the QE hypothesis in order to increase the QE purity of the sample. Such a selection will remove events modified by FSI or caused by non-QE processes. The presented QE-like analysis specifically retains sensitivity to these effects by requiring only that the final-state proton's direction

and momentum be measured.

Presented is a differential cross-section measurement of QE-like events that consist of a muon with at least one proton and no pions in the final state. By using the kinetic energy of the most energetic (leading) proton, a measurement of Q^2 is made from the hadronic component alone. This extracted cross section is measured with much improved acceptance at large muon scattering angles and higher Q^2 than that of MINERvA's QE measurements that rely on muon kinematics [7, 8].

The MINERvA detector [31] is comprised of a fine-grained scintillator central tracking region surrounded by electromagnetic and hadronic calorimeters. The core consists of tracking planes made of interleaved scintillator strips of triangular profile, enabling charged-particle energy depositions to be located to within 3 mm. The planes are mounted vertically, nearly perpendicular to the neutrino beam axis which is 58 mrad from horizontal. Three different plane orientations ($0°$ and $\pm60°$ from the vertical) permit three-dimensional reconstruction of charged particle trajectories. The detector's 3 ns hit-time resolution allows separation of multiple neutrino interactions within each 10 μs spill from the accelerator. The scintillator planes are supported by exterior hexagonal steel frames with rectangular scintillator bars embedded into slots, which serve as the side hadronic calorimeter. The magnetized MINOS near detector [32] located two meters downstream of MINERvA serves as a muon spectrometer.

These data were taken in the NuMI beamline at Fermilab when its focusing elements were configured to produce an intense beam of muon neutrinos (ν_μ) peaked at 3.5 GeV. The run period for these data occurred between March 2010 and April 2012, and corresponds to 3.04×10^{20} protons on target (POT). The neutrino flux is over 95% ν_μ in the peak, with the remainder consisting of $\bar{\nu}_\mu$, ν_e, and $\bar{\nu}_e$, and is predicted using a GEANT4-based model constrained by hadron production data [33] as described in Ref. [34].

Neutrino interactions are simulated using the GENIE 2.6.2 [35] event generator. The propagation of particles in the detector and the corresponding detector response are simulated with GEANT4 [36]. The calorimetric energy scale is tuned using through-going muons to ensure that the photon statistics and reconstructed energy deposition agree between simulation and data. Measurements made with a smaller version of the MINERvA detector in a low energy hadron test beam [31] are used to constrain the uncertainties associated with the detector response to both protons and charged pions.

For each QE-like candidate, a muon and at least one proton are reconstructed as tracks, where the proton track originates from the most upstream position of the muon track. This selection includes all muons that exit either the side of the central tracking region or the downstream end. Therefore, the selection has good acceptance for events with muon scattering angles up to $70°$ relative to the beam direction. Events are required to occur at

—————————

†now at SLAC National Accelerator Laboratory, Stanford, California 94309 USA
‡also at Department of Physics, University of Antananarivo, Madagascar
§also at Institute of Theoretical Physics, Wrocław University, Wrocław, Poland
¶now at Argonne National Laboratory, Argonne, IL 60439, USA

least 22 cm from the edge of the scintillator and within the central 110 planes of the tracking region, defining a fiducial region of 5.57 metric tons. For 53% of the events, the muon track is matched to a track in the MINOS detector, allowing the charge and momentum to be determined. An additional 8% of muons entering MINOS are not tracked there. As for the muons that exit the MINERvA outer calorimeter, only a lower-bound on the momentum is obtained. A minimum of five distinct energy depositions is required to form a proton track, resulting in a 110 MeV kinetic energy threshold. The proton tracks must stop in the inner region of MINERvA.

Particle identification (PID) and the reconstructed energy for protons are determined using a track-based dE/dx algorithm. The algorithm fits the measured dE/dx profile of a track to predicted profiles for both proton and pion hypotheses, and the two fit χ^2 values are used to construct a proton PID consistency score [37]. This fitting routine successfully identifies protons that rescatter due to nuclear interactions and provides a kinetic energy resolution of 5% for all identified protons. An event is retained if all non-muon tracks pass a cut on the proton PID consistency score.

The remaining cuts are designed to remove inelastic background events with an untracked pion. Pions with kinetic energies above 100 MeV are likely to interact strongly within the detector materials, produce hadronic showers, and consequently are unable to be reconstructed as tracks. These events are removed by cutting on energy E_{extra} that is not linked to a track and is located outside of a 10 cm sphere centered at the vertex. Excluding this vertex region when making this cut reduces sensitivity to mismodeling of low energy nucleons [7, 8], which may arise from FSI or multinucleon effects. Pions with kinetic energies below 100 MeV are removed using an algorithm that identifies Michel electrons from the $\pi \to \mu \to e$ decay chain occurring near the vertex at a delayed time relative to the initial neutrino interaction. After applying all cuts, the sample contains 40,102 QE-like candidates. The simulation predicts that 34.5% of the events are from backgrounds containing at least one final-state pion, where the backgrounds are described below.

Measurement of the proton angle and momentum provides several variables that are sensitive to FSI. One variable is the angle φ between the ν-muon and ν-proton planes, and is shown in Fig. 1 for both the data and two simulations: one with FSI and one without FSI. For both simulations, the non-QE-like background is tuned using a data-based procedure described below. For QE scattering off a free neutron at rest $\varphi = 180°$. The detector resolution on φ is 3.8 degrees, so the width shown on the distributions in Fig. 1 is due to Fermi motion, inelastic scattering, and FSI effects. The comparison shows that GENIE with FSI describes the data better than GENIE without FSI. The remaining discrepancy suggests additional FSI or cross section effects not present in the GENIE simulation.
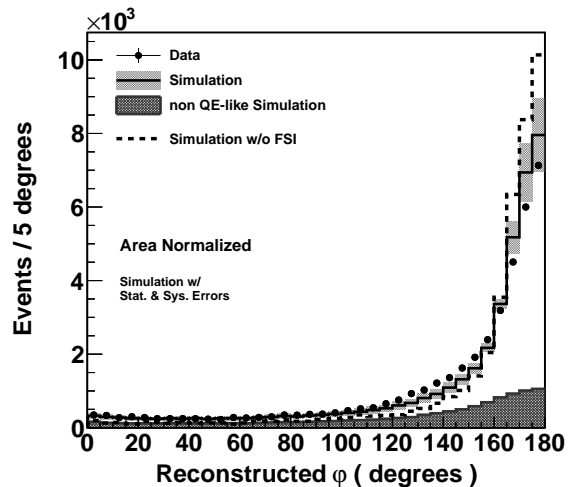

FIG. 1: Angle between the ν-muon and ν-proton planes for data (black points) and two predictions from GENIE, where the solid line prediction includes FSI and the dashed line prediction does not. The total predictions have been normalized to the data, and the non-QE-like predictions have been normalized to sidebands in the data.

The differential cross section $d\sigma/dQ^2$ is measured using the leading proton and the assumption of QE scattering from a neutron at rest. Under this assumption, Q^2 is given by

$$Q^2_{QE,p} = (M_n - \epsilon_B)^2 - M_p^2 + 2(M_n - \epsilon_B)(T_p + M_p - M_n + \epsilon_B),$$

where T_p is the kinetic energy of the proton, $M_{n,p}$ is the nucleon mass, and ϵ_B is the effective binding energy of +34 MeV [38]. This estimation of $Q^2_{QE,p}$ depends only on the T_p of the leading proton. This approximation of $Q^2_{QE,p}$ deviates from the Q^2 estimated using only the muon. For the QE-like signal events that pass the analysis cuts, Fig. 2 shows GENIE's average values of various estimates of Q^2 using truth information as a function of Q^2 as defined by the muon kinematics, namely:

$$Q^2_{QE,\mu} = -m_\mu^2 + 2E_\nu(E_\mu - \sqrt{(E_\mu^2 - m_\mu^2)} \cos\theta_\mu),$$

where E_μ, θ_μ, and m_μ are the true energy, true scattering angle, and mass of the muon and E_ν is the true energy of the neutrino. The solid and short-dashed curves show $Q^2_{QE,\mu}$ from the muon, and the discrepancy at $Q^2_{QE,\mu} > 1.7$ GeV^2 is from differences in the way the neutrino energy is estimated. The solid curve uses the neutrino's true energy, and short-dashed curve uses the QE hypothesis to estimate the neutrino energy using the muon's true energy and angle, which is given by

$$E_{QE,\nu} = \frac{2(M_n - \epsilon_B)E_\mu - [(M_n - \epsilon_B)^2 + m_\mu^2 - M_p^2]}{2(M_n - \epsilon_B - E_\mu + \sqrt{(E_\mu^2 - m_\mu^2)} \cos\theta_\mu)}.$$

At higher $Q^2_{QE,\mu}$, the QE hypothesis inaccurately describes the inelastic component of the QE-like signal.

The dotted and long-dashed curves show $Q^2_{QE,p}$ from the proton, and the effects of FSI contribute to the discrepancy between the curves. The tracking threshold prevents the reconstruction of events with a leading proton having $T_p < 110$ MeV, thereby resulting in a $Q^2_{QE,p}$ limit roughly 0.2 GeV^2 and poor acceptance for $Q^2_{QE,\mu} < 0.2$ GeV^2. Based on the Bodek-Ritchie [39, 40] prescription, GENIE models the momentum distribution of initial-state nucleons by including a high-momentum tail extending beyond the Fermi momentum. Consequently at low $Q^2_{QE,\mu}$, the analysis preferentially selects events where the initial-state nucleon momentum is greater than the Fermi momentum. This is a feature of the proton-based curves in Fig. 2. The differences between the muon-based and proton-based estimates come from Fermi motion for the dotted curve and Fermi motion with FSI for the long-dashed curve, where such nuclear effects distort the shape of the $Q^2_{QE,p}$ distribution.
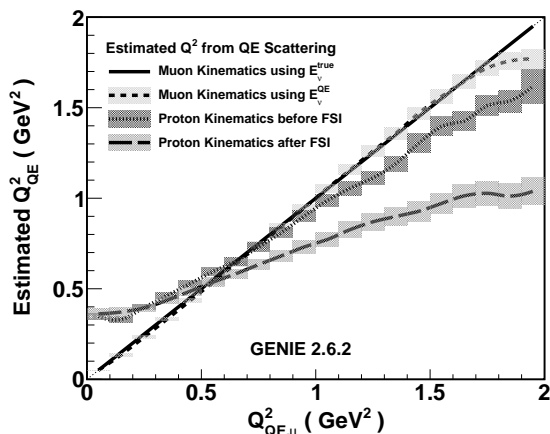

FIG. 3: Distribution of Q^2 of the QE-like events determined by the leading proton track reconstruction in data and simulation, where the background estimates are tuned to sideband samples of the data.

FIG. 2: Comparisons between several Q^2 estimates as function of the Q^2 estimated using muon kinematics for the QE-like signal events that pass the reconstruction and analysis cuts, as described in the text. The error bands include statistical and GENIE systematic uncertainties.

The reconstructed $Q^2_{QE,p}$ distribution is shown in Fig. 3. The data are compared to GENIE predictions of the QE-like signal and backgrounds, where the background estimates have been tuned using the data. The largest background comes from baryon resonance production, predominantly $\Delta(1232)$. A smaller background originates from non-resonant inelastic pion production, which is referred to as deep-inelastic scattering (DIS) in GENIE. In the tuning procedure, the non-QE-like backgrounds are categorized as one of two processes: "resonant" or "DIS plus other" (hereafter denoted DIS+), where the "other" includes $\overline{\nu}_\mu$ interactions and a smaller neutral current component. Four distinct sideband regions of the E_{extra} distribution are used to extract normalization constants for each process. The sidebands further from the signal region are predicted to contain a larger estimated fraction of DIS+ relative to the reso-
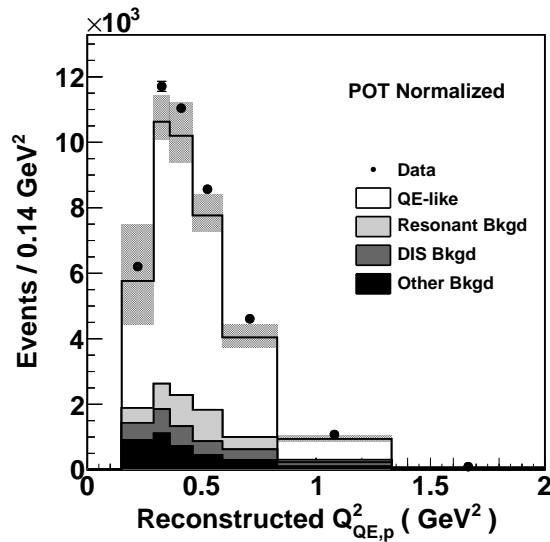
nant fraction and are more consistent with the data. By separating the simulated backgrounds into two processes, the backgrounds in each $Q^2_{QE,p}$ bin are determined from a linear fit that simultaneously matches the simulated background to data in all sideband regions. The tuning results indicate that the baryon resonance production background should be reduced by roughly 50%. The DIS+ background prediction remains nearly unchanged for $Q^2_{QE,p} > 0.5$ GeV^2 and increases by $20-60\%$ in $Q^2_{QE,p}$ regions between 0.15 to 0.5 GeV^2.

After subtracting the data-tuned backgrounds, the yield is corrected for detector smearing of the leading proton energy via a Bayesian unfolding procedure using four iterations [41]. The simulation is used to correct for geometric acceptance and efficiency for the unfolded distribution. To obtain the flux-averaged differential cross section, the yields are divided by the number of nucleons in the fiducial volume (3.294×10^{30}) and the integrated ν_μ flux below 100 GeV (3.286×10^{-8}/cm^2/POT).

The systematic uncertainties on $d\sigma/dQ^2_{QE,p}$ arise from imperfect knowledge of the (I) neutrino beam flux, (II) neutrino interactions, (III) final state interactions, (IV) detector energy response, (V) hadron inelastic cross sections, and (VI) other sources, and are listed in Table I. Most uncertainties are evaluated by randomly varying the associated parameters in the simulation within uncertainties and re-extracting $d\sigma/dQ^2_{QE,p}$. Each variation is normalized to the measured $d\sigma/dQ^2_{QE,p}$ to extract the uncertainty in the shape. Consequently, in regions where the shape of the $d\sigma/dQ^2_{QE,p}$ changes dramatically, the uncertainty on the shape may exceed that of the absolute uncertainty.

The uncertainty on the beam flux affects the normalization of $d\sigma/dQ^2_{QE,p}$ and is correlated across $Q^2_{QE,p}$ bins. The uncertainties on the neutrino interaction and FSI models affect $d\sigma/dQ^2_{QE,p}$ through the efficiency correction and are dominated by uncertainties on the resonance production axial mass parameter, pion absorption, and pion inelastic scattering. The uncertainties associated with hadron propagation through MINERvA are evaluated by shifting the pion and proton total inelastic cross sections by 10%, an uncertainty derived from external hadron production data [42–45]. This uncertainty affects proton tracking and PID efficiencies and acceptance for $Q^2_{QE,p} > 0.8$ GeV^2. The systematic uncertainty from the detector energy response is relatively small and is dominated by uncertainties on the reconstruction of the proton and E_{extra}.

TABLE I: Fractional systematic uncertainties (in units of percent) on $d\sigma/dQ^2_{QE,p}$ for each $Q^2_{QE,p}$ bin, with contributions from (I) neutrino beam flux, (II) neutrino interaction models, (III) final-state interaction models, (IV) detector energy response, (V) hadronic inelastic cross section model, and (VI) other sources. The absolute uncertainties are followed by the shape uncertainties in parentheses.

$Q^2_{QE,p}$ (GeV^2)	I	II	III	IV	V	VI	Total
0.15 - 0.29	7.2(0.6)	5.3(6.6)	4.3(11)	3.0(3.9)	2.0(3.4)	2.9(1.6)	11(14)
0.29 - 0.36	7.6(0.2)	5.8(3.1)	7.3(1.5)	1.3(1.7)	3.2(4.7)	2.6(1.4)	13(6.3)
0.36 - 0.46	7.5(0.4)	7.5(2.0)	11(3.2)	2.0(1.1)	3.3(3.3)	1.1(0.3)	16(5.1)
0.46 - 0.59	7.7(0.2)	8.8(2.4)	13(4.3)	2.9(1.1)	2.0(0.8)	1.0(0.5)	17(5.1)
0.59 - 0.83	8.0(0.3)	9.6(3.1)	13(4.3)	4.1(2.1)	1.6(0.9)	1.0(0.6)	18(5.9)
0.83 - 1.33	8.2(0.6)	10(3.4)	12(3.3)	7.5(5.6)	9.6(8)	1.4(2.1)	21(11)
1.33 - 2.00	8.2(0.7)	11(4.3)	11(2.4)	7.8(7.5)	3.8(3.2)	1.9(1.2)	19(9.6)

The QE-like differential cross section[1] as a function of $Q^2_{QE,p}$ is shown in Fig. 4 (top), along with predictions from the GENIE and NuWro [46, 47] generators using a RFG model. Several extensions to the NuWro QE RFG prediction are shown, inspired by measurements based on lepton kinematics. Each prediction represents the sum over all reactions with at least one >110 MeV proton and no pions in the final state. The inelastic contributions to this QE-like cross section from the GENIE (dark dashed) and NuWro (light dashed) predictions are shown, and differ in both rate and shape. For both generators, the inelastic component is dominated by $\Delta(1232)$ production and decay, where the pion is absorbed by the residual nucleus.

The shape of $d\sigma/dQ^2_{QE,p}$ can be compared between prediction and data with reduced systematic uncertainty by normalizing each prediction to the data. Figure 4 (bottom) shows the ratio between the data and normalized prediction to the GENIE RFG prediction. For both the absolute and the shape comparisons, the χ^2 between the data and each prediction, including correlations between bins, is given in Table II. The highest $Q^2_{QE,p}$ data point contributes mostly to the total χ^2 for the GENIE RFG and NuWro RFG with RPA+Nieves. The remaining predictions get most of their total χ^2 from the middle data points, which have higher and positive covariance values, but these predictions visibly have an opposite trend to the data.
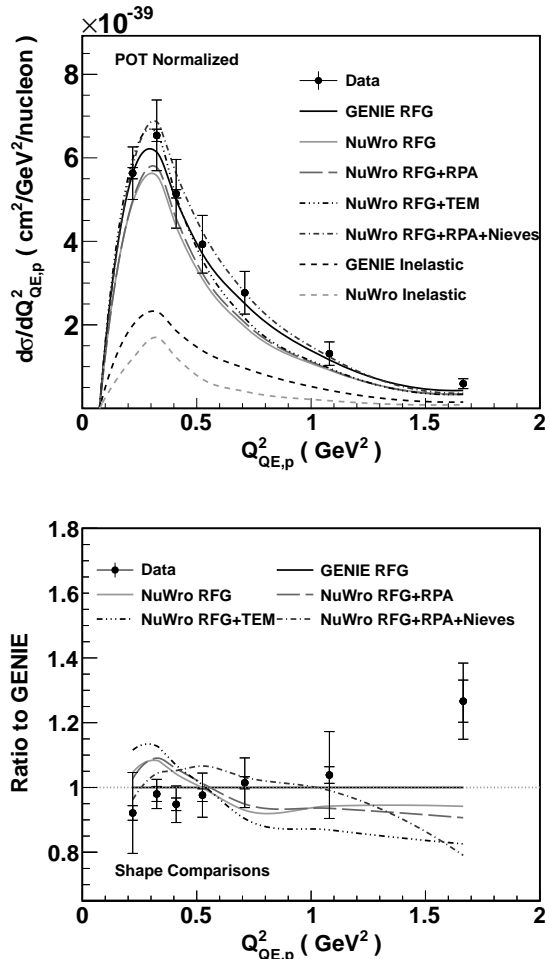

FIG. 4: (Top) QE-like cross section versus $Q^2_{QE,p}$ compared to several different predictions, along with the GENIE (dark dashed line) and NuWro (light dashed line) predictions of the inelastic contribution to the QE-like prediction. (Bottom) Ratio between the data and predictions to the GENIE RFG prediction including the inelastic component, where all models are normalized to the data. The inner (outer) error bars correspond to the statistical (total) uncertainties.

The rate and shape of the data are best described by the GENIE RFG model with the inelastic component, followed by the NuWro RFG model with its very different prediction of the inelastic process. The remaining NuWro predictions become more discrepant with the shape of the data, as various implementations of nuclear effects are incorporated.

GENIE and NuWro calculate QE scattering using

_____

[1] See at URL for $d\sigma/dQ^2_{QE,p}$ numerical values.

the independent nucleon impulse approximation, the BBBA2005 parameterization [48] of the vector form factors, and an axial mass of 0.99 GeV/c^2. As described above, GENIE has in addition an approximation of short-range correlations included as prescribed by Bodek-Ritchie [39, 40].

TABLE II: Calculated χ^2 between the data and various models with M$_A$ = 0.99 GeV/c^2. The number of degrees of freedom is 7 (6) for the rate (shape).

Model	Rate χ^2	Shape χ^2
GENIE RFG	8.5	10.8
NuWro RFG	12.2	19.9
NuWro RFG + RPA	13.5	21.7
NuWro RFG + RPA + Nieves	25.9	28.5
NuWro RFG + TEM	27.6	34.5

The difference between GENIE and NuWro RFG predictions arises primarily in the difference between the two simulations' treatments of inelastic scattering. In GENIE, resonance production is defined using the formalism of Rein-Sehgal [49] while in NuWro, it is defined as interactions with invariant hadronic mass $W < 1.6$ GeV, and where contributions come from $\Delta(1232)$ excitations. GENIE and NuWro handle interactions with $W > 1.6$ GeV similarly and transport hadrons through the nucleus using different implementations of an intranuclear cascade model.

RPA calculations predict a suppression of the cross section at very low Q^2 from long-range correlations, and enhancement at moderate Q^2 due to short-range correlations. For the NuWro RPA calculation [12], the suppression happens below MINERvA's proton kinetic energy threshold, and its curve is nearly identical to NuWro RFG prediction as shown in Fig. 4. MEC between nucleons enhance the cross section and populate the transition region between the QE and Δ peaks. MEC are part of both the microscopic model of Nieves [13, 21] and the Transverse Enhancement Model (TEM) which is empirically extracted from electron scattering data [18]. TEM is based on QE lepton kinematics so that the energy transfer follows from reweighting QE events rather than filling the transition region between the QE and Δ peaks, while the Nieves model gives systematically higher energy transfers which translate to an enhancement at higher proton energies. The proton kinematics are not explicitly calculated in either the TEM or the Nieves model, and in NuWro are assigned as described in Refs. [20, 47].

The agreement between the presented QE-like data and the GENIE prediction is in stark contrast to that of the MINERvA QE measurements [7, 8], where Q^2 is based on muon kinematics and the backgrounds from
[2] See at URL for the $d\sigma/dQ^2_{QE,\mu}$ values as a function of $Q^2_{QE,\mu}$.

all inelastic events are subtracted. To check the consistency between MINERvA muon-based QE and proton-based QE-like measurements, the subsample of events with muons that are tracked in MINOS is used to measure the pure QE differential cross section^2 as a function of Q^2 estimated from the muon kinematics as given in Ref [8]. These results are consistent with the reported QE measurement [8] while using a factor of three more protons on target but lower acceptance because of the proton track requirement.

The inconsistency of the models of the hadronic and leptonic aspects of the QE-like sample may be resolved by modifying the $\Delta(1232)$ production cross section and nuclear absorption models. Supporting evidence comes from the results of the background tuning described above and MINERvA's inclusive pion production measurement [34],which finds Δ-dominated single pion production to be nearly 30% less than the GENIE prediction. Refinements to models of multinucleon effects, beyond those implemented in these versions of GENIE and NuWro, may also resolve the discrepancies seen here.

This proton-based $d\sigma/dQ^2_{QE,p}$ measurement provides a new way to evaluate the modeling of all contributions to the QE-like cross section, and finds that the models which best describe the proton kinematics of this interaction differ from those that best describe the muon kinematics. The models used by neutrino oscillation experiments must ultimately reproduce the hadronic as well as leptonic kinematics since both affect neutrino energy reconstruction.

[1] R. Gran *et al.* (K2K Collaboration), Phys. Rev. D **74**, 052002 (2006), arXiv:0603034 [hep-ex] .

[2] A. A. Aguilar-Arevalo *et al.* (MiniBooNE Collaboration),

Phys. Rev. Lett. **100**, 032301 (2008), arXiv:0706.0926 [hep-ex] .

[3] X. Espinal and F. Sanchez, AIP Conf. Proc. **967**, 117 (2007).

[4] V. Lyubushkin *et al.* (NOMAD Collaboration), Eur. Phys. J. C **63**, 355 (2009), arXiv:0812.4543 [hep-ex] .

[5] Y. Nakajima (SciBooNE Collaboration), AIP Conf. Proc. **1405**, 47 (2011).

[6] A. A. Aguilar-Arevalo *et al.* (MiniBooNE Collaboration), Phys. Rev. D **88**, 032001 (2013), arXiv:1301.7067 [hep-ex] .

[7] L. Fields *et al.* (MINERvA Collaboration), Phys. Rev. Lett. **111**, 022501 (2013), arXiv:1305.2234 [hep-ex] .

[8] G. Fiorentini *et al.* (MINERvA Collaboration), Phys. Rev. Lett. **111**, 022502 (2013), arXiv:1305.2243 [hep-ex] .

[9] O. Benhar, D. Day, and I. Sick, Rev. Mod. Phys. **80**, 189 (2008), arXiv:0603029 [nucl-ex] .

[10] J. Arrington, D. Higinbotham, G. Rosner, and M. Sargsian, Prog. Part. Nucl. Phys. **67**, 898 (2012), arXiv:1104.1196 [nucl-ex] .

[11] J. Arrington, A. Daniel, D. Day, N. Fomin, D. Gaskell, *et al.*, Phys. Rev. C **86**, 065204 (2012), arXiv:1206.6343 [nucl-ex] .

[12] K. M. Graczyk and J. T. Sobczyk, Eur. Phys. J. C **31**, 177 (2003), arXiv:0303054 [nucl-th] .

[13] J. Nieves, J. E. Amaro, and M. Valverde, Phys. Rev. C **70**, 055503 (2004), arXiv:0408005 [nucl-th] .

[14] M. Valverde, J. E. Amaro, J. Nieves, and C. Maieron, Phys. Lett. B **642**, 218 (2006), arXiv:0606042 [nucl-th] .

[15] M. Martini, M. Ericson, G. Chanfray, and J. Marteau, Phys. Rev. C **80**, 065501 (2009), arXiv:0910.2622 [nucl-th] .

[16] M. Martini, M. Ericson, G. Chanfray, and J. Marteau, Phys. Rev. C **81**, 045502 (2010), arXiv:1002.4538 [hep-ph] .

[17] J. Nieves, I. Ruiz Simo, and M. J. Vicente Vacas, Phys. Rev. C **83**, 045501 (2011), arXiv:1102.2777 [hep-ph] .

[18] A. Bodek, H. S. Budd, and M. E. Christy, Eur. Phys. J. C **71**, 1726 (2011), arXiv:1106.0340 [hep-ph] .

[19] G. Shen, L. E. Marcucci, J. Carlson, S. Gandolfi, and R. Schiavilla, Phys. Rev. C **86**, 035503 (2012), arXiv:1205.4337 [nucl-th] .

[20] J. T. Sobczyk, Phys. Rev. C **86**, 015504 (2012), arXiv:1201.3673 [hep-ph] .

[21] R. Gran, J. Nieves, F. Sanchez, and M. Vicente Vacas, Phys. Rev. D **88**, 113007 (2013), arXiv:1307.8105 [hep-ph] .

[22] T. Leitner and U. Mosel, Phys. Rev. C **81**, 064614 (2010), arXiv:1004.4433 [nucl-th] .

[23] M. Martini, M. Ericson, and G. Chanfray, Phys. Rev. D **85**, 093012 (2011), arXiv:1202.4745 [hep-ph] .

[24] M. Martini, M. Ericson, and G. Chanfray, Phys. Rev. D **87**, 013009 (2013), arXiv:1211.1523 [hep-ph] .

[25] J. Nieves, F. Sanchez, I. Ruiz Simo, and M. J. Vicente Vacas, Phys. Rev. D **85**, 113008 (2012), arXiv:1204.5404 [hep-ph] .

[26] O. Lalakulich, K. Gallmeister, and U. Mosel, Phys. Rev. C **86**, 014607 (2012), arXiv:1205.1061 [nucl-th].

[27] O. Lalakulich, U. Mosel, and K. Gallmeister, Phys. Rev. C **86**, 054606 (2012), arXiv:1208.3678 [nucl-th] .

[28] U. Mosel, O. Lalakulich, and K. Gallmeister, Phys. Rev. Lett. **112**, 151802 (2014), arXiv:1311.7288 [nucl-th] .

[29] C. Adams *et al.* (LBNE Collaboration), (2013), arXiv:1307.7335 [hep-ex].

[30] F. Jedin (NOvA), J. Phys. Conf. Ser. **490**, 012019 (2014).

[31] L. Aliaga *et al.* (MINERvA Collaboration), Nucl. Instrum. Methods in Phys. Res., Sect. A **743**, 130 (2014), arXiv:1305.5199 [physics.ins-det].

[32] D. G. Michael *et al.* (MINOS Collaboration), Nucl. Instrum. Meth. A **596**, 190 (2008), arXiv:0805.3170 [physics.ins-det] .

[33] C. Alt *et al.* (NA49 Collaboration), Eur. Phys. J. C **49**, 897 (2007), arXiv:0606028 [hep-ex] .

[34] B. Eberly *et al.* (The MINERvA Collaboration), (2014), arXiv:1406.6415 [hep-ex].

[35] C. Andreopoulos *et al.* (GENIE Collaboration), Nucl. Instrum. Meth. A **614**, 87 (2009), arXiv:0905.2517 [hep-ph].

[36] S. Agostinelli *et al.* (GEANT4), Nucl. Instrum. Meth. A **506**, 250 (2003).

[37] T. Walton, *A Measurement of the Muon Neutrino Charged Current Quasielastic-like Cross Section on a Hydrocarbon Target and Final State Interaction Effects*, Ph.D. thesis, Hampton University. (2014).

[38] E. J. Moniz, I. Sick, R. R. Whitney, J. R. Ficenec, R. D. Kephart, *et al.*, Phys. Rev. Lett. **26**, 445 (1971).

[39] A. Bodek and J. L. Ritchie, Phys. Rev. D **23**, 1070 (1981).

[40] A. Bodek and J. L. Ritchie, Phys. Rev. D **24**, 1400 (1981).

[41] G. D'Agostini, Nucl. Instrum. Meth. A **362**, 487 (1995).

[42] T. Lee and R. Redwine, Ann. Rev. Nucl. Part. Sci. **52**, 23 (2002).

[43] D. Ashery, I. Navon, G. Azuelos, H. Walter, H. Pfeiffer, *et al.*, Phys. Rev. C **23**, 2173 (1981).

[44] B. Allardyce, C. Batty, D. Baugh, E. Friedman, G. Heymann, *et al.*, Nucl. Phys. A **209**, 1 (1973).

[45] A. Saunders, S. Hoeibraten, J. Kraushaar, B. Kriss, R. Peterson, *et al.*, Phys. Rev. C **53**, 1745 (1996).

[46] J. A. Nowak and J. T. Sobczyk, Acta Phys. Polon. B **37**, 2371 (2006), arXiv:0608108 [hep-ph] .

[47] T. Golan, K. M. Graczyk, C. Juszczak, and J. T. Sobczyk, Phys. Rev. C **88**, 024612 (2013), arXiv:1302.3890 [hep-ph] .

[48] R. Bradford, A. Bodek, H. S. Budd, and J. Arrington, Nucl. Phys. Proc. Suppl. **159**, 127 (2006), arXiv:0602017 [hep-ex] .

[49] D. Rein and L. M. Sehgal, Annals Phys. **133**, 79 (1981).